Journal of South American Earth Sciences 98 (2020) 102442

Contents lists available at ScienceDirect

Journal of South American Earth Sciences

journal homepage: www.elsevier.com/locate/jsames

Paleomagnetic evidence of the brittle deformation of the Central Patagonian Batholith at Gastre area (Chubut Province, Argentina)

Víctor Ruiz González[a,*], Carla G. Puigdomenech[a], Claudia B. Zaffarana[b], Haroldo Vizán[a], Rubén Somoza[a]

[a] IGEBA, UBA, CONICET, Argentina
[b] IIPG, UNRN, CONICET, Argentina

ARTICLE INFO

Keywords:
Gastre Fault System
Andean Orogeny
Tectonic inversion
Gastre Basin

ABSTRACT

The Central Patagonian Batholith (CPB) in the Gastre area, central Patagonia, constitutes a set of two I-type Late Triassic plutonic suites, the Gastre superunit with a U-Pb zircon age of 221 ± 2 Ma, and the Lipetrén superunit with a U-Pb SHRIMP age of 215 ± 1 Ma. The source of this calc-alkaline batholith is characterized by crustal and mantle contributions, and it registers NW-SE subvertical magmatic and solid-state fabrics. These features, together with its intraplate position away from the inferred proto-Gondwana margin, have made it the focus of different tectonic interpretations. Early studies have interpreted it as the record of major dextral motions along the transcontinental NW-SE-striking Gastre fault system in Jurassic times. Later interpretations have proposed that the magmatic and tectonic foliations of the CPB were formed during a sinistral transpressive regime which was aided by Late Paleozoic widespread NW-SE subvertical structures in the North Patagonian Massif. Paleomagnetism, a unique tool to detect the presence of tectonic block rotations on vertical axes, was applied in the CPB in order to constrain the timing and type of deformation in the area. A paleomagnetic pole was obtained, which statistical parameters are: N = 45, Lat. = 81.4°S, Long. = 207°E, K = 11.5, A95 = 6.6°. Although the position of this pole does not coincide with equivalent Late Triassic poles, this position can be reconciled with the presence of a NE tilting of about 11° of the sampled block of the batholith. The tilting would have been aided by the NW-SE subvertical structures that affect the area. These paleomagnetic results rule out the possibility of vertical axis rotations from Late Triassic to present times and suggest that the ductile syn- to post-emplacement deformation of the CPB in Gastre area occurred during this period (Late Triassic), being the later brittle deformation triggered by the Andean Orogeny a possible explanation for this tilting.

1. Introduction

The Central Patagonian Batholith (CPB; Fig. 1) was originally defined as extensive Late Triassic calc-alkaline plutonic suite aligned in an NW-SE direction, in the central-southern sector of the North Patagonian Massif from Gastre to Pilcaniyeu (Rapela et al., 1991, 1992; Rapela and Kay, 1988). Both, the CPB and its metamorphic host rocks, are affected by a low-temperature solid-state deformation event which originated the presence of tectonic NW-SE subvertical foliations of variable intensity degree, which were originally described as "Gastre system" by Coira et al. (1975). The CPB is located in an inland position with respect to the proto-Gondwana margin, and it represents a key element in paleogeographic models of pre-Gondwana breakup, as it was emplaced during the transition of the Gonwanide (Late Paleozoic) and the Andean (Jurassic to present) orogenic cycles in South America. It has a geochemical signature intermediate between mantle and crustal magmas (Rapela et al., 1991, 1992; Rapela and Pankhurst, 1992). The Late Triassic magmas of CPB have been recently proposed by Navarrete et al. (2019) as part of an inland magmatic arc.

Early studies of the CPB in its type area interpreted it as intruded syn-kinematically within a transcontinental NW-SE dextral shear zone named "Gastre Fault System" (Rapela et al., 1991, 1992), a useful tool widely invoked to restore Patagonia to achieve a tectono-stratigraphic correlation between the Paleozoic successions from the Malvinas-Falkland islands and the Cape fold belt of South Africa (Hole et al., 2016; MacDonald et al., 2003; Marshall, 1994; Storey et al., 1999). However, mesoscale observations in the type locality of the Gastre fault were against the idea of Jurassic dextral transcontinental faults

* Corresponding author. Instituto de Geociencias Básicas, Aplicadas y Ambientales de Buenos Aires (UBA - CONICET), Facultad de Ciencias Exáctas y Naturales, Universidad de Buenos Aires, Intendente Güiraldes 2160, CABA, Argentina.
E-mail address: vruizgonzalez@gl.fcen.uba.ar (V. Ruiz González).

https://doi.org/10.1016/j.jsames.2019.102442
Received 8 October 2019; Received in revised form 24 November 2019; Accepted 24 November 2019
Available online 28 November 2019
0895-9811/

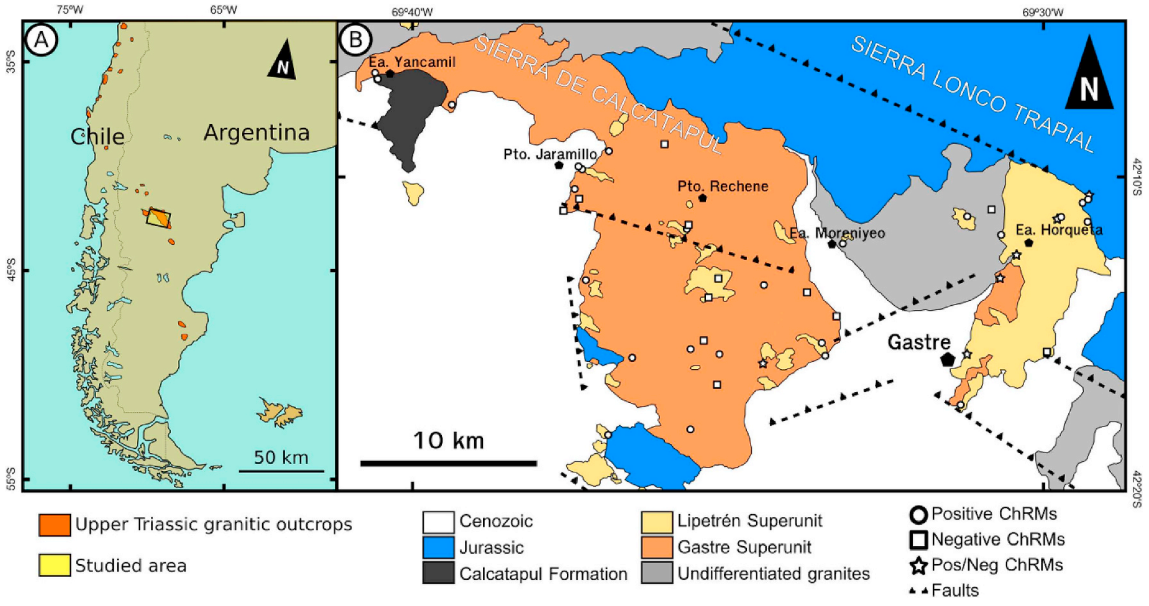

Fig. 1. Map of the studied area. A) Regional map of the CPB, with its type locality near Gastre and the correlated outcrops further south in the Deaseado Massif (modified from Navarrete et al., 2019). B) Geological map of the study area modified from Zaffarana et al. (2017) integrating some structural features from Bilmes et al. (2014). Sites with samples showing positive polarities are plotted with circles, those showing negative polarities are plotted with squares, and those with both, positive and negative polarities, plotted with a star.

traversing the Gastre area (von Gosen and Loske, 2004; Zaffarana et al., 2010, 2014). Furthermore, the results of a paleomagnetic study from the overlying Lonco Trapial Formation indicated that no clockwise tectonic rotations took place in the Jurassic through the Gastre area (Zaffarana and Somoza, 2012). The internal structure of the CPB was mapped using anisotropy of magnetic susceptibility (AMS), a study which led to the definition of a pattern of NW-SE subvertical magmatic and tectonic fabrics, interpreted as produced by a syn-tectonic emplacement within a sinistral transpressive regime (Zaffarana et al., 2017). This work uses the same dense grid of sampling sites of that previous AMS study of the CPB in order to study its deformation from the paleomagnetic point of view. Paleomagnetism, as a unique tool able to recognize tectonic block rotations in the vertical axis, is a fundamental method to unravel kinematics of shear zones. The paleomagnetic pole calculated in this study contributes to the discussion about the timing and style of deformation of this area of the North Patagonian Massif.

2. Geological setting

2.1. Local geology

In its type locality in the area of Gastre, the CPB has an excellent exposure, where it is composed of two superunits: the older Gastre Superunit and the younger Lipetrén Superunit (Fig. 1). The oldest intrusive rocks are the equigranular hornblende-biotite granodiorites (EHBG) which gradually pass to the porphyritic biotite-hornblende monzogranites (PBHM, Zaffarana et al., 2014). The Gastre Superunit is also composed of stocks of equigranular biotitic monzogranites (EBM), stocks of dioritic to quartz-monzodioritic composition and dikes of dioritic to quartz-dioritic composition (HQD-stocks and HQD-dikes, Zaffarana et al., 2014). The dioritic to quartz-dioritic dikes intrude all the previous units of the Gastre Superunit. The younger Lipetrén Superunit, in turn, forms stocks and dikes of biotitic monzo- and syenogranites (BG) which intrude the Gastre Superunit. The Lipetrén Superunit also comprises the Horqueta Granodiorite (HG, Rapela et al., 1991, 1992), a set of granites and granodiorites bearing biotite as their main mafic mineral.

The Gastre Superunit has a U-Pb zircon age of 221 ± 2 Ma (age mentioned in Rapela et al. (2005) without providing analytical data) and an Rb-Sr age of 222 ± 3 Ma (Rapela et al., 1992); isochrons recalculated by Zaffarana et al. (2014). The Gastre Superunit also has a ^{40}Ar-^{39}Ar stepwise biotite cooling age of 213 ± 15 Ma (Zaffarana et al., 2014). The Lipetrén Superunit has a U-Pb SHRIMP (sensitive high-resolution ion microprobe) zircon age of 215 ± 1 Ma (Lagorio et al., 2015), and a ^{40}Ar-^{39}Ar stepwise biotite cooling age of 206 ± 4 Ma (Zaffarana et al., 2014). The Horqueta Granodiorite has a U-Pb zircon SHRIMP crystallization age of 213 ± 2 Ma (Lagorio et al., 2015), which partly overlaps with the ^{40}Ar-^{39}Ar stepwise biotite cooling age of 211 ± 2 Ma (Zaffarana et al., 2014).

The oldest rocks intruded by the CPB are the Early Paleozoic phyllites, quartzite layers, (injected) micaschists, amphibolites, gneisses and migmatites of the Cushamen Formation, which are mostly exposed north of the study area (López de Luchi and Cerredo, 2008; Volkheimer, 1964). However, a small septum of metamorphic rocks was recognized in the Gastre area and was ascribed to this formation (Zaffarana et al., 2012). The CPB is mainly hosted by the Late Paleozoic Calcatapul Formation (Nullo, 1978; Proserpio, 1978), a metamorphic succession of acidic and basic metavolcanic rocks along with thin layers of phyllites and lenses of metaconglomerates (von Gosen and Loske, 2004; Zaffarana et al., 2010). The CPB is also hosted by a granitic suite belonging to an earlier, Late Paleozoic-Early Mesozoic intrusive cycle represented in the Gastre area by the Sierra del Medio and the Laguna del Toro granites (Lagorio et al., 2015; Rapela et al., 1992), together with the Yancamil Granite (von Gosen and Loske, 2004). More regionally, this previous intrusive cycle is represented by the Mamil Choique Formation (Cerredo and lópez de Luchi, 1998; López de Luchi and Cerredo, 2008), which crops out towards the NNW of the area of study, in the Mamil Choique area. The CPB is covered by the Early to Middle Jurassic volcanic rocks of Lonco Trapial Formation (Page and Page, 1994; Zaffarana et al., 2018a).

2.2. Deformation of the CPB in the context of the North Patagonian Massif

The analysis of microstructures and magnetic foliation data of the CPB in Gastre demonstrate that its emplacement would have occurred syn-tectonically with a transpressive deformation regime (Zaffarana et al., 2017). The patron of the magmatic as well as the solid-state foliations of the granites are subparallel, defining a trend of NW-SE

subvertical structures. Within the North Patagonian Massif, there are NW-SE trending subvertical structures which would constitute its structural grain, inherited from the pervasive Late Paleozoic deformation (Álvarez et al., 2014; Giacosa et al., 2004, 2014; 2017; Renda et al., 2019; von Gosen et al., 2002; Gosen, 2009; von Gosen and Loske, 2004).

As mentioned before, the existence of the "Gastre Fault System" as a transcontinental, dextral transcurrent, fault system has been dismissed by several authors (Franzese and Martino, 1998; von Gosen and Loske, 2004; Zaffarana et al., 2010, 2017; Zaffarana and Somoza, 2012). These structures were analyzed in detail by von Gosen and Loske (2004), and later they were reviewed by Zaffarana et al. (2010), to which they added more evidence (Zaffarana et al., 2017). All the studied structures have directions and senses of deformation different from each other, without showing a clear predominance of the deformations by any of them. However, it is true that the most prominent fractures are NW-SE, but these have the same direction of the previous Paleozoic structures, which were the hosts of the intrusion of the granites that make up the batholith, acquiring a sub-parallel fabric (Zaffarana et al., 2010, 2017).

3. Analytical procedure

3.1. Sampling method, rock magnetism and demagnetization

This work presents the paleomagnetic measurements of the same AMS sites reported by Zaffarana et al. (2017). The sampling method was designed to fit for both kinds of studies (at least five different samples were obtained from each sampling site). The collection of 1219 oriented cores belongs to 149 stations (Zaffarana et al., 2017, and references therein). From those samples, 240 were studied for paleomagnetic proposes, of which, 100 had interpretable paleomagnetic behavior and belonged to the CPB units.

The complete study of rock magnetism of the sampled units is shown in Zaffarana (2011) and in Zaffarana et al. (2017). The presence of titanomagnetite and low titanium magnetite is deduced in the different facies of the Gastre Superunit. Hematite was also detected in the Lipetrén Superunit. It should also be noted that, in all the facies of the CPB, there are pseudo-single domain magnetites and titanomagnetites along with multidomain magnetites (Zaffarana, 2011).

Magnetic remanences were measured with a 2G cryogenic magnetometer in the Paleomagnetism Laboratory "Daniel A. Valencio" of the IGeBA (UBA-CONICET). The thermal demagnetizations were carried out by an ASC furnace and alternating fields (AF) demagnetizations were done with the static demagnetizer attached to a 2G magnetometer. AGICO "Remasoft" software was used to analyze the magnetic behaviors of the samples and determine the characteristic remanent magnetizations (ChRM).

3.2. Analysis and validation of the paleomagnetic data

The ChRMs were determined only in their geographic corrections due to the lack of paleohorizontal evidence. However, this correction is accepted as "in situ" due to their magnetic fabric coincidence with the host rock fabrics (Zaffarana et al., 2012, 2017). Remanence directions (ChRM) with less than 15° of Maximum Angular Deviation (MAD) calculated using at least 3 demagnetization steps were exclusively accepted for the analysis (Kirschvink, 1980). Samples with less than 30% of the NRM intensity after steps of 20 mT or 300 °C of demagnetization were discarded, considering that low coercivities (Hc) or low unblocking temperatures could belong to spurious magnetic components (Fig. 2). In each sampling site, there are different lithologies, corresponding to the CPB forming magmatic event (Table 1). These samples are not strictly coeval neither within a site nor between sites. Therefore, the paleomagnetic analysis was performed using the ChRMs of the samples without averaging them per site, according to Deenen et al. (2011), and the whole sampling area was considered as belonging to the same tectonic block (Fig. 1). Many of the rejected samples (55/100) were very unstable, probably because their magnetization was dominated by multi-domain magnetite (Zaffarana, 2011).

Virtual Geomagnetic Poles (VGPs) were calculated from each ChRM (Fig. 3), and a cut-off angle of 40° was applied to the VGPs to filter transitional and spurious data (Wilson et al., 1972). In order to validate these results, a reversal test was carried out with the ChRM directions corresponding to the VGPs inside the cut off angle. The reversal test was positive with C classification, a Critical Gamma of 10.93 and an Observed Gamma of 1.89 (McFadden and McElhinny, 1990). This test implies that the demagnetization was successful in defining the primary magnetization of the CPB and proves that the paleosecular variation

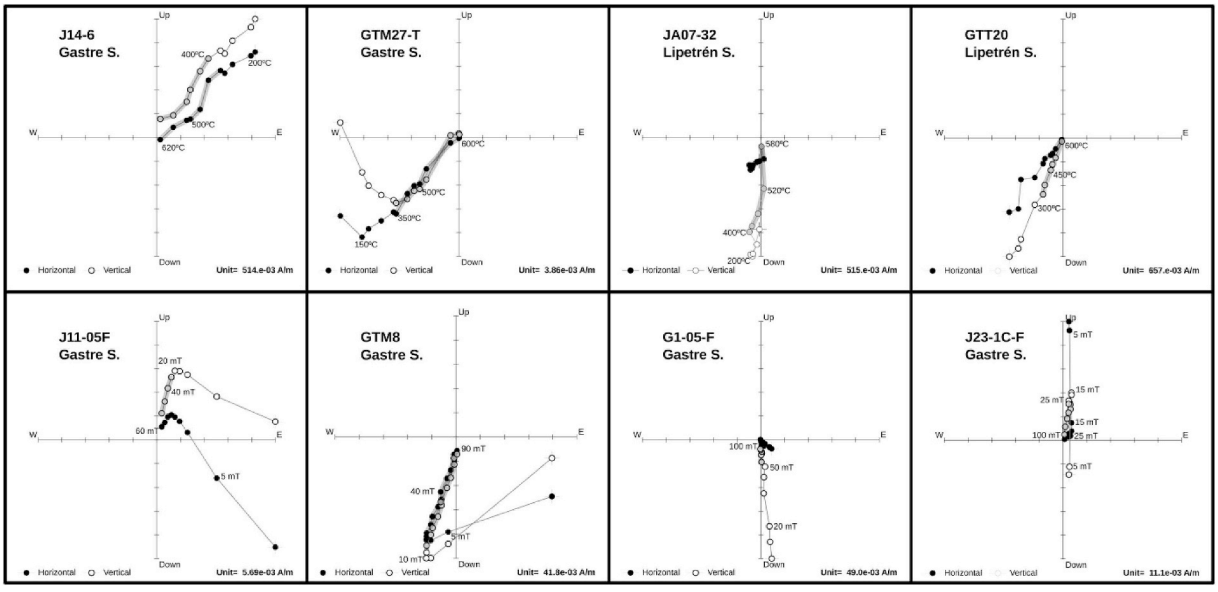

Fig. 2. Zijderveld diagrams showing the ChRMs (in gray) of demagnetized samples using alternate fields (up) and thermal method (down), also positive and negative directions are shown.

Table 1
Geographic coordinates of each site, ChRM of samples with their MAD and calculated VGPs. Below, normal and reverse mean directions with their statistical parameters (Fisher, 1953). Those samples, from which VGPs that are inside the 40° window, are highlighted in gray. Sites with * where not used for the AMS study.

Unit		AMS Site	Sample	Lat. (N)	Long. (E)	Dec.	Inc.	MAD	VGP Lat.	VGP Long.
Magmatic fabrics ("M" type)										
Gastre Superunit	Equigranular hornblende-biotite granodiorites (EHBG)	P168-V	JA07.15C	-42.1724	-69.4169	264.6	33.8	11.2	-16.21	-148.9
		P172-V	A5-1	-42.1900	-69.1460	57.9	10.4	12	19.31	-5.78
			A5-2A	-42.1900	-69.1460	130.9	19.4	7.2	-36.46	43.11
		P175	JA07.43B	-42.2233	-69.3171	319.9	36.7	6.6	17.22	-108.51
		P63	JA0722-B	-42.1522	-69.3987	265.5	23.5	3.5	-11.5	-153.19
		P65	G14,4B	-42.1872	-69.2095	210.4	50.9	1.6	-63.67	187.09
		P73	A4-4B	-42.1800	-69.1490	166.8	63.3	2.5	-80.08	0.88
		P28	J23-1C-F	-42.2754	-69.3415	59.1	-77.7	4.5	-50.22	-101.76
			J23.2B	-42.2754	-69.3415	89.6	-68.5	3.7	-32.11	-116.28
		P31	gty2	-42.2621	-69.3865	140.5	67	10.6	-61.92	-8.4
		P33	J0730-1-	-42.2208	-69.4111	206.3	78.8	7.8	-60.37	-88.68
		P37	J10-6-T	-42.2649	-69.3177	98.8	-84.4	10.4	-39.66	-83.62
			J10-05-T	-42.2649	-69.3177	208.7	-80.3	5	-25.24	-59.43
			J10-07-T	-42.2649	-69.3177	274.9	-74.2	4.7	-38.06	-30.76
			J10-9-T	-42.2649	-69.3177	354.7	85.9	4.1	-34.14	-70.23
			J10-8-T	-42.2649	-69.3177	357.6	78.4	1.8	-19.96	-70.29
			J10-01-T	-42.2649	-69.3177	279.6	59.2	1.5	-19.73	-122.69
		P39	J13-06-T	-42.2400	-69.2787	207.5	-2.2	8.3	40.06	-32.18
		P44	J0730-12	-42.1601	-69.4153	170	57.1	8	-81.14	47.48
			J0730-14	-42.1601	-69.4153	177.2	69.4	4.6	-78.93	-60.62
			J0730-13	-42.1601	-69.4153	185.9	72.4	7.4	-74.11	-81.02
			J0730-11	-42.1601	-69.4153	135.8	74.9	8	-57.46	-31.42
		GTP*	GTP6	-42.2200	-69.1922	152.9	55.5	5.6	-68.19	28.24
	Porphyritic biotite-hornblende monzogranites (PBHM)	P51	G1-05-F	-42.1274	-69.4819	172.1	74.8	9.5	-70.07	-58.38
		P81	E4-2B	-42.2590	-69.3410	219.5	57.1	2.4	-59.67	-154.57
		P35	J12-04F	-42.2573	-69.3558	51.7	78.5	10.4	-26.74	-50.01
			J12-3F	-42.2573	-69.3558	258.4	82.6	9.2	-43.49	-89.2
		P166	E4-4	-42.2590	-69.3410	241	77.4	1.2	-49.5	-102.68
	Equigranular biotitic monzogranites (EBM)	P171-V	A1-23A	-42.3000	-69.3560	17.4	44.7	11	19.52	-52.83
			A1-22C	-42.3000	-69.3560	81.3	47.8	10.3	-13.12	-6.63
	Hornblende quartz-diorites (HQD)-dikes	P95	J11-06F	-42.2527	-69.3486	29.8	-65.6	1.7	-68.37	-134.29
			J11-05F	-42.2527	-69.3486	29.6	-64.9	2.9	-68.55	-136.77
		P98	A7-14D	-42.2541	-69.2865	152.7	12.8	1	-46.84	68.94
		GTP*	gtp1t	-42.2200	-69.1922	348.3	-50.6	0.8	-75.66	66.43
			gtp4t	-42.2200	-69.1922	44.4	-38.6	4.8	-47.78	186.03
			gtp2t	-42.2200	-69.1922	53.3	-74.1	5.3	-53.41	-110.94
			gtp3t	-42.2200	-69.1922	173.1	57.8	2.8	-83.53	54.17
			gtp5t	-42.2200	-69.1922	346	-63.6	1.1	-79.46	-0.41
Lipetrén Superunit	Biotitic granites (BG)	P4	GTH4-AF	-42.1885	-69.1621	204.8	56.6	2.7	-70.34	194.34
			GTH1T	-42.1885	-69.1621	17.2	59.4	2.9	6.14	-56.03
			GTH2T	-42.1885	-69.1621	197.8	62.8	4.5	-76.89	-144.25
		P6	gtl4	-42.1948	-69.1719	232.7	-53.8	4.3	-0.47	-28.11
			GTL1TT	-42.1948	-69.1719	173.9	-42.9	7.3	22.65	-75.17
			GTL08	-42.1948	-69.1719	201.2	-13.2	12.1	37.43	-42.28
			GTL9	-42.1948	-69.1719	293.3	-1.9	6.6	-17.71	36.25
			GTL7TT	-42.1948	-69.1719	134.8	10	9.6	-35.38	50.72
			GTL6	-42.1948	-69.1719	358.1	30.7	9.5	31.24	-71.3
			gtg5af	-42.1948	-69.1719	233.1	33	12.4	-39.09	189.33
			GTL10	-42.1948	-69.1719	41.9	41.2	4.7	13.64	-30.16
			GTL05	-42.1948	-69.1719	60	60.1	5.3	-9.28	-27.71
		P8	GTF03	-42.2076	-69.1836	147.6	-10.3	3.5	34.2	-109.36
			GTF4	-42.2076	-69.1836	196.1	-3.7	3.9	43.6	-46.68
			GTF05	-42.2076	-69.1836	218.4	-1.5	7.1	34.87	-19.99
			GTF01	-42.2076	-69.1836	121.9	-0.7	12.4	22.79	-136.23
			GTF02	-42.2076	-69.1836	147.8	6	9.6	-41.39	65.64
		P105	JA07.6B	-42.1837	-69.4225	323.8	-59.9	9.8	-63.05	11.23
		P107	JA07-19	-42.1617	-69.4129	344.3	26.8	8.3	31.84	-87.4
		P111	JA07.29C	-42.3030	-69.3992	72.7	77.8	4.5	-32.04	-42.85
		P112	J0701.3-B	-42.2047	-69.2752	243.2	-10.5	7.2	15.7	-1.87
			JA07-32	-42.2047	-69.2752	200.9	73.1	6.3	-68.98	-100.37
		P120	G5.2A	-42.2591	-69.1674	318	-56	4.7	-57.39	16.65
		P127	G10,3A	-42.1967	-69.1917	199.5	52.1	7.8	-71.91	175.57
		P128	A8-1B	-42.2300	-69.3460	111.6	-34.4	8.8	2.3	-131.03
		P129	A9-1A	-42.2200	-69.3410	120.8	-62.3	3.4	-10.88	-108.64
		G11*	G11.2	-42.1833	-69.1967	195.3	-56	10.8	10.04	-56.76
		P152	J8.3A	-42.2609	-69.2846	135.4	41.4	5.2	-48.89	32.98
	Horqueta granodiorite	P1	GTI01	-42.1876	-69.1600	312.2	-65	4.9	-56.16	-4.03
			GTI4	-42.1876	-69.1600	135	-9.4	11.4	27.82	-121.99
			GTI3TT	-42.1876	-69.1600	296.8	4.1	7.9	18.05	-138.91
		P2	GTJ5	-42.1831	-69.1525	62.4	27.1	5.7	9.56	-8.62
Superimposition of low-temperature solid-state deformation ("S" type)										
Gastre supersunit	Equigranular hornblende-biotite granodiorites (EHBG)	P144	J14-7F3	-42.2274	-69.2943	9.5	-56.7	2.8	-81.19	169.69
			J0701.21A	-42.2274	-69.2943	352.6	-54.8	5.7	-81.01	68.42
			J14.6	-42.2274	-69.2943	45.1	-45.4	11	-50.36	192.75
			J14-1b-F	-42.2274	-69.2943	352.5	-20.6	0.9	-57.74	96.8
			J070119-A	-42.2274	-69.2943	176.5	23.7	2.2	-60	103.86
	Porphyritic biotite-hornblende monzogranites (PBHM)	P47	J21-5-T	-42.1486	-69.3693	22.5	-24.8	6.4	-54.93	151.09
	Hornblende quartz-diorites (HQD)-stocks	P15	GTM20-T	-42.2600	-69.2140	60.3	-77.5	8.6	-49.77	-102.24
			GTM27-T	-42.2600	-69.2140	220.9	38.9	6.2	-50.39	183.03
			gtm4af	-42.2600	-69.2140	183.9	40.2	3.8	-70.37	121.54
			gtm3af	-42.2600	-69.2140	184.4	38.3	4.3	-68.96	122.25
			gtm5	-42.2600	-69.2140	55.1	18.3	1.3	17.94	-10.94
			GTM1-T	-42.2600	-69.2140	173	44.1	11	-72.61	89.25
			GTM14-T	-42.2600	-69.2140	177.3	46.1	3.5	-75.03	101.47
			GTM8	-42.2600	-69.2140	197.9	46.6	2.8	-69.54	161.82
			GTM17-T	-42.2600	-69.2140	205.9	48.9	4.2	-65.79	178.31
		P90	9F03F	-42.1918	-69.3566	352.3	-70.6	6.1	-76.38	-50.23
			2a	-42.1918	-69.3566	300.4	64.5	10.9	-13.13	-107.04
	Hornblende quartz-diorites (HQD)-dikes	P101	G07.17C	-42.1777	-69.4144	0.1	-56.8	6.3	-85.2	111.54
Lipetrén supersunit	Biotitic Granites (BG)	P114	JA07.50B	-42.1918	-69.3566	72.2	-43.4	12.7	-29.46	-150.7
		P14	GTA7	-42.2600	-69.2140	135.7	14.7	9	-37.78	49.6
			gtm32	-42.2600	-69.2140	22.3	-64.4	11.9	-73.6	-137.62
			GTM31-T	-42.2600	-69.2140	220.9	37.8	14.5	-49.88	182.11
		P59 (Gastre mylonites-N)	O604	-42.2600	-69.2140	283.2	-46.6	12.7	-27.63	7.06
			O614	-42.2600	-69.2140	137.7	25	5.2	-43.3	46.55
			0601B	-42.2600	-69.2140	68.2	48.1	8.6	-5.01	-14.71
			O618	-42.2600	-69.2140	193.1	60.8	5.7	-80.27	-157.41
		P20 (Gastre mylonites-S)	GTT3	-42.2865	-69.2135	305.8	-27.7	7.6	-36.11	34.6
			GTT17	-42.2865	-69.2135	296.4	-27.2	3.4	-29.08	27.73
			GTT27	-42.2865	-69.2135	96.1	-17.4	5.6	-1.52	-148.54
			GTT20	-42.2865	-69.2135	219.5	58.6	4.3	-60.22	-151.44

Paleomagnetic Pole				N	Dec.	Inc.	R	k	a95
P. Lat. (S)	P. Long. (E)	K	A95	28	190.6	58.6	26.6	19.3	6.4
81.4	207	11.5	6.6	17	13.6	-59.7	15.9	14.2	9.8
				45	191.7	59.1	42.5	17.4	5.3

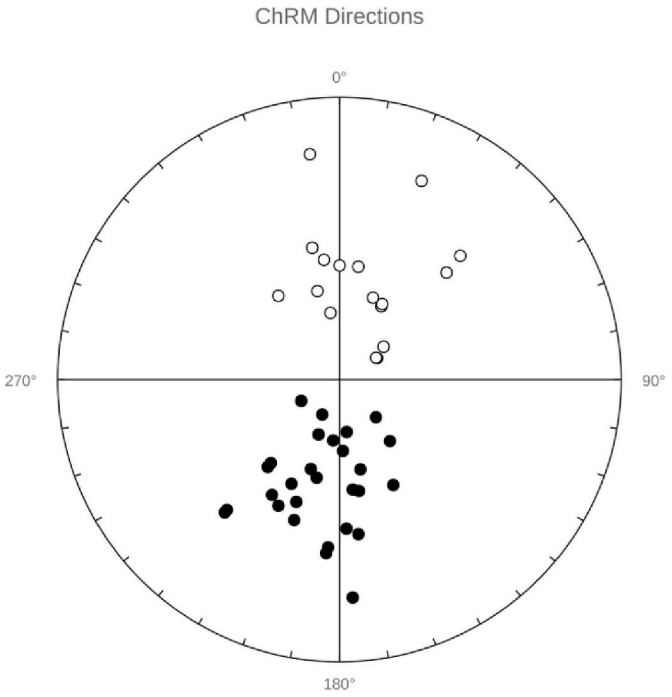

Fig. 3. Stereographic projection of positive (filled dots) and negative (empty dots) Characteristic Remanent Magnetizations relative to the VGPs within a 40° cut-off angle.

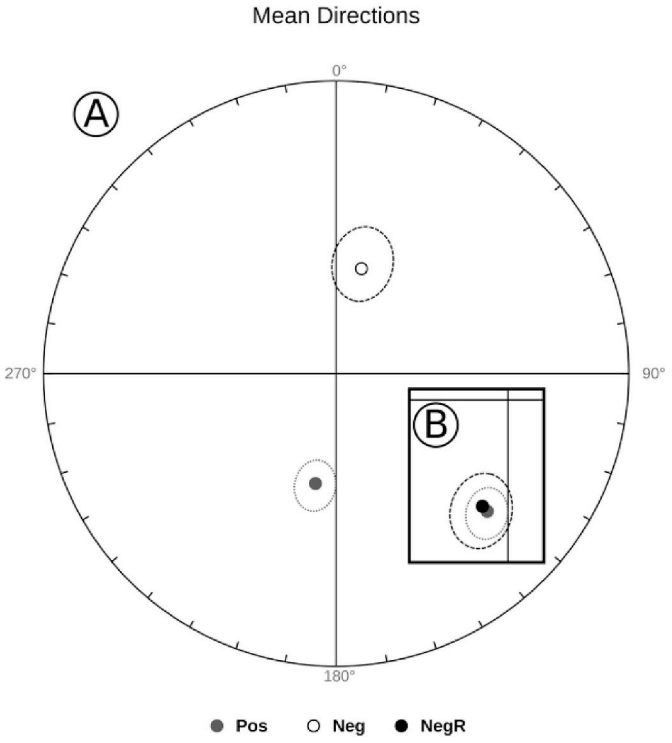

Fig. 4. Stereographic projection of the mean values of the ChRM directions: A) normal and reverse means, and B) both means in reverse polarity (positive).

was averaged (Fig. 4). A paleomagnetic pole was calculated re-calculating the mean VGP directions to a reference point near the center of the sampling area (Lat: 42.2°S; Long: 69.3°E). The statistical parameters of this paleomagnetic pole are: N = 45, Lat. = 81.4°S, Long. = 207°E, K = 11.5, A95 = 6.6° (Fig. 5).

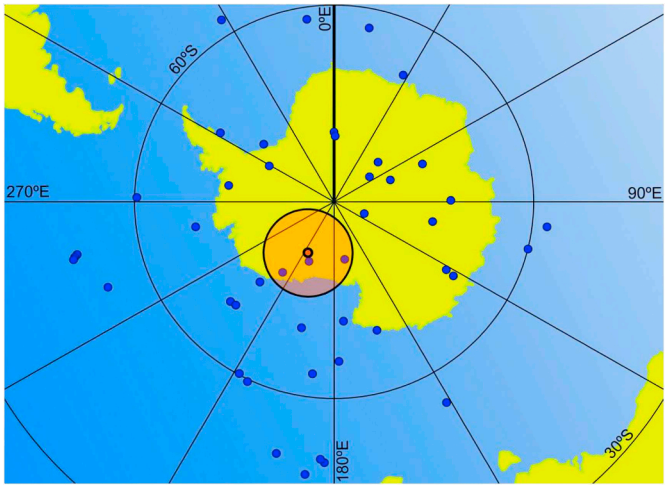

Fig. 5. Calculated paleomagnetic pole with its A95° (orange dot and oval) and VGPs within a 40° cut-off angle (blue dots). (For interpretation of the references to colour in this figure legend, the reader is referred to the Web version of this article.)

4. Discussion

In order to analyze the dynamics recorded by the remanent magnetic directions, integrated in the paleomagnetic pole shown in this work, it is necessary to compare it with other paleopoles of the same age. For this purpose, the global average poles calculated by Kent and Irving (2010) and Torsvik et al. (2012) for 210 Ma, transported to South American coordinates through the translations proposed in those works, and also, the paleomagnetic pole calculated for the Norian by Vizán et al. (2004) for the Upper Triassic rocks from Los Colorados hills in Mendoza, were used (Fig. 6). The paleomagnetic pole calculated for the Central Patagonian Batholith is close to the South American average for 180 Ma (Ruiz González et al., 2019), as can be seen in Fig. 6. So that, as mentioned before, the "Gastre Fault System" was proposed for the Early Jurassic. Then, if these structures had acted during that time, ChRMs recorded in the rocks would show a Jurassic age, due to a pervasive remagnetization of the materials. But the existence of positive and negative remanent directions of the samples, and the unreseted ages calculated with the ^{40}Ar-^{39}Ar method by Zaffarana et al. (2014) and Lagorio et al. (2015) strongly suggest that the magnetizations are primary and that they were not remagnetized during Jurassic times.

As explained by Zaffarana et al. (2017), magmatic fabrics and low-temperature solid-state fabrics are pervasive throughout the granite bodies of the CPB. Sites with magmatic as well as solid-state fabrics are part of the calculated paleomagnetic pole (see Table 1), showing no difference in the ChRMs between sites with different deformation styles. This implies that the ChRMS of magmatic fabric sites and the ChRMs of the low-temperature solid-state fabric sites coincide due to the brief time elapsing between both events, and it also implies that both events happened over the Curie temperature of magnetite (580 °C; Dunlop and Özdemir, 1997) and close to the Néel temperature of hematite (675 °C; O'Reilly, 1984). The coincidence in remanent directions of both fabrics implies that the remanence was acquired during the Late Triassic after the granitic rocks cooled. In addition, as shown in Zaffarana et al. (2012), the Jurassic rocks of the Lonco Trapial Formation appear undeformed overriding the granites of the CPB. This also corroborates, together with the remanence directions registered in the CPB, that the deformation described in Zaffarana et al. (2017) did not occur during the Jurassic.

Therefore, as the remanence registered in the CPB rocks was acquired after the cooling of the batholith and the rocks were not

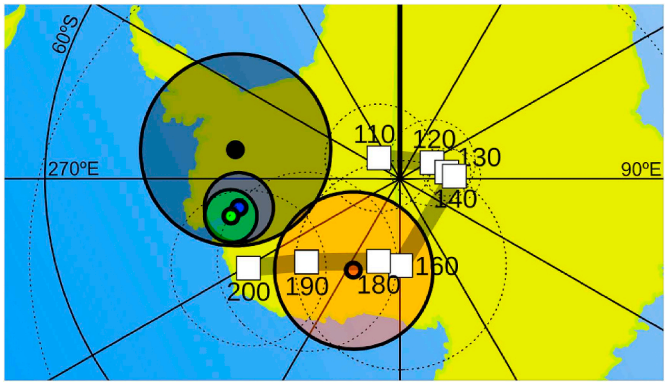

Fig. 6. Central Patagonian Batholith paleomagnetic pole in orange, Los Colorados paleomagnetic pole in black (Vizán et al., 2004), 210 Ma global mean paleomagnetic pole by Kent and Irving (2010) in blue, 210 Ma global mean paleomagnetic pole by Torsvik et al. (2012) in green, and South American APW path modified from Ruiz González et al. (2019) in white squares. All paleomagnetic poles are plotted in South American coordinates. (For interpretation of the references to colour in this figure legend, the reader is referred to the Web version of this article.)

remagnetized after the Late Triassic, the next step is to characterize the possible deformation for the area since Late Triassic times. When a possible tectonic motion of the analyzed block is calculated with the correlative Late Triassic poles, a vertical rotation is discarded (see Table 2). When the CPB paleopole is compared with the pole of Vizán et al. (2004), the uncertainty is greater than the proposed rotation, which implies that, if it exists, it would not be detectable by comparing these two poles. Besides, when the CPB paleopole is compared with those of Kent and Irving (2010) and Torsvik et al. (2012) the rotation is less than one degree, and its uncertainty is much higher than the calculated rotation (see Table 2).

However, it shows a possible latitudinal displacement towards the geomagnetic pole of the tectonic block of about 12°. Nevertheless, this cannot be possible because it strongly contradicts the paleogeographic configuration of southwestern Gondwana during the Late Triassic (Hervé et al., 2008; Suárez et al., 2019; Vizán et al., 2017). Then, a tectonic event could have affected the batholith and produce the tilting of the block, during the Jurassic extensional period (Figari, 2005) and, or, during a compressional stage, during the Late Cretaceous or later, related to the Andean Orogeny (Bilmes et al., 2013, 2014; Savignano et al., 2016; Zaffarana et al., 2018b). The main fractures in the Gastre area show a NW-SE direction and could have been originated during the formation of the Cañadón Asfalto Basin (Figari, 2005), where they acted as normal faults (part of half grabens), probably developed aided by the previous Paleozoic structures (Renda et al., 2019). This set of semi-parallel fractures are also proposed to have acted as reverse faults during the Late Cretaceous and, or, Miocene, triggered by the Andean Orogeny, during the formation of the Gastre Basin (Bilmes et al., 2013, 2014; Savignano et al., 2016).

Two paleomagnetic studies determined the presence of vertical axis rotation of tectonic blocks during Jurassic times in the southwestern area of the North Patagonian Massif. One was performed in the Early Jurassic Lonco Trapial Formation, in the outcrops immediately in the north of the studied area, on the rocks overlying the CPB granites (Zaffarana and Somoza, 2012), whereas the other study was carried out south to the Gastre area, in the middle course of the Chubut River (Geuna et al., 2000), in the Late Jurassic Cañadón Asfalto Formation. The Lonco Trapial Formation blocks show counterclockwise vertical rotation of ~20°, which implies a possible sinistral shear sense. In turn, the Cañadón Asfalto Formation paleopole shows a vertical clockwise rotation of ~30° of the studied area, which implies a possible dextral shear sense. Hence, these studies show that the northern and southern areas from the studied block report different senses of vertical axes rotation during Jurassic times, but, in the southern block is recorded an absence of vertical rotations since the Early Cretaceous (Geuna et al., 2000). This context implies that the whole area suffered a complex dynamic deformation during Jurassic times, synchronically with the development of the Cañadón Asfalto Basin (Giacosa et al., 2004, 2014; 2017). However, this deformation had not affected, apparently, the Central Patagonian Batholith at Gastre, as was proposed by Aragón et al. (2011) in an analogous case: a body with the size and rigidity as the CPB could have remained undeformed, while extensive stresses were distributed between units of smaller thickness and cohesion, to the north and south with opposite senses.

The formation of the Gastre Basin during the Andean Orogeny (Late Cretaceous to Miocene times) could have affected the structural stability of the studied block, because even the granitic body of the CPB could have been tilted around 11° towards the NE, reactivating previous Paleozoic structures that could have aided or channeled this deformation. These compressive efforts must have been of greater magnitude than those related to the Jurassic extension, generating the creation (aided by Paleozoic foliation) of inverse faults or reversing the normal Jurassic faults (Savignano et al., 2016). Probably, the deformation of the La Pava Formation during the Middle Miocene (Bilmes et al., 2014) was associated with these displacements, recording an inclination similar to the proposed for the studied block in this work.

Table 2
Statistical parameters comparing the calculated paleomagnetic pole of the CPB with the reference poles.

Tectonic Motions	CPB pole	Los Colorados (Vizán et al., 2004)	210 Ma Global Mean (Torsvik et al., 2012)	210 Ma Global Mean (Kent and Irving, 2010)
Latitude (N)	−81.4	−76	−75.5	−76.3
Longitude (E)	207	280	257.5	259.8
Pole A95	6.6	8	2.2	2.9
Pole N	45	12	41	11
Poleward Displacement		13.4 ± 7.6	11.1 ± 5.1	10.9 ± 5.3
Apparent Rotation		7.0 ± 12.4	1.7 ± 7.1	0.1 ± 7.5
Bedding correction	CPB pole	Los Colorados (Vizán et al., 2004)	210 Ma Global Mean (Torsvik et al., 2012)	210 Ma Global Mean (Kent and Irving, 2010)
Declination	191.7	184.6	193.4	191.8
Inclination	59.1	71.3	69.8	69.7
Strike/Dip		293.2/12.6	278.2/10.7	281.5/10.6

5. Conclusions

The development of the fractures and lineaments of the so-called "Gastre Fault System" has, possibly, its origin in the fabric inherited from the Late Paleozoic, a set of structures with an NW-SE direction. These same structures would have facilitated the intrusion of the granite bodies that formed the CPB during the Late Triassic, making the fabric of these granites to be subparallel to these Paleozoic structures. The paleomagnetic pole obtained in this work was defined by rocks bearing magmatic, high-temperature and low-temperature solid-state deformation. This constraints the magmatic and solid-state deformation events to Late Triassic times during the emplacement and cooling of the batholith. The intrusion of the granites of the CPB generated local deformations within the batholith, with different kinematics, directions and senses. After the cooling of the CBP, during the Early Jurassic the depocenters of the Cañadón Asfalto Basin began to form, generating normal faults throughout the area. The formation of those faults and their complex kinematics could have triggered the rotation and tilting of blocks. By the Early Cretaceous these depocenters were filled, and the rotations of the tectonic blocks ceased. Finally, due to the stresses associated with the Andean Orogeny in the studied area, the inherited Paleozoic foliation of the CPB and, or, the discontinuities and fractures generated during the opening of the Cañadón Asfalto Basin would have helped the development of reverse faulting. One of these structures responsible for the tectonic inversion could have generated the tilting towards the NE of 11°, which was observed in the tectonic block of the CPB studied in this work.

Acknowledgements

This work was partially funded by doctoral scholarship PICT 1074-2006 from Agencia Nacional de Promoción Científica y Tecnológica and by PIP 02828 project from Consejo Nacional de Investigaciones Científicas y Técnicas.

We would like to thank Emiliano Renda for his support during this work, to Carmen Martínez Dopico for her advice, and Leandro Gallo for his help and constructive and inspiring discussions. We dedicate this work to our colleague, mentor, and friend Rubén Somoza, without whom none of this would have been possible. We also would like to give thanks to the editor, Andrés Folguera, and the two anonymous reviewers of this work.

Appendix A. Supplementary data

Supplementary data to this article can be found online at https://doi.org/10.1016/j.jsames.2019.102442.

References

Álvarez, D., Peroni, J., Giacosa, R., Silva Nieto, D., Busteros, A., Lagorio, S.L., 2014. Evidencias magnetométricas de las estructuras andinas y prea-andinas en Gastre y Cushamen (41° 30′– 43° 00′ S, SO del Macizo Norpatagónico). In: XIX Congreso Geológico Argentino. Asociación Geológica Argentina, Córdoba.

Aragón, E., D'Eramo, F., Castro, A., Pinotti, L., Brunelli, D., Rabbia, O., Rivalenti, G., Varela, R., Spakman, W., Demartis, M., Cavarozzi, C.E., Aguilera, Y.E., Mazzucchelli, M., Ribot, A., 2011. Tectono-magmatic response to major convergence changes in the North Patagonian suprasubduction system; the Paleogene subduction–transcurrent plate margin transition. Tectonophysics 509, 218–237. https://doi.org/10.1016/j.tecto.2011.06.012.

Bilmes, A., D'Elia, L., Veiga, G.D., Franzese, J.R., 2014. Relleno intermontano en el Antepaís Fragmentado Patagónico: evolución neógena de la Cuenca de Gastre. Rev. Asoc. Geol. Argent. 71, 311–330.

Bilmes, A., D'Elia, L., Franzese, J.R., Veiga, G.D., Hernández, M., 2013. Miocene block uplift and basin formation in the Patagonian foreland: the Gastre Basin, Argentina. Tectonophysics 601, 98–111. https://doi.org/10.1016/j.tecto.2013.05.001.

Cerredo, M.E., lópez de Luchi, M.G., 1998. Mamil Choique Granitoids, southwestern North Patagonian Massif, Argentina: magmatism and metamorphism associated with a polyphasic evolution. J. South Am. Earth Sci. 11, 499–515. https://doi.org/10.1016/S0895-9811(98)00025-X.

Coira, B., Nullo, F., Proserpio, C., Ramos, V., 1975. Tectónica de Basamento de la Región Occidental del Macizo Nordpatagónico (provincias de Río Negro y del Chubut), vol. 30. pp. 361–383.

Deenen, M.H.L., Langereis, C.G., van Hinsbergen, D.J.J., Biggin, A.J., 2011. Geomagnetic secular variation and the statistics of palaeomagnetic directions. Geophys. J. Int. 186, 509–520. https://doi.org/10.1111/j.1365-246X.2011.05050.x.

Dunlop, D.J., Özdemir, Ö., 1997. Rock Magnetism: Fundamentals and Frontiers. Camb. Core. https://doi.org/10.1017/CBO9780511612794.

Figari, E.G., 2005. Evolución tectónica de la cuenca de Cañadón Asfalto (zona del Valle Medio del Río Chubut). Universidad de Buenos Aires, Buenos Aires.

Fisher, R.A., 1953. Dispersion on a sphere. Proc. R. Soc. Lond. A 217, 295–305. https://doi.org/10.1098/rspa.1953.0064.

Franzese, J., Martino, R.D., 1998. Aspectos cinemáticos y tectónicos de la zona de cizalla de Gastre en la Sierra de Calcatapul, Provincia de Chubut, Argentina. In: X Congreso Latinoamericano de Geología. Presented at the X Congreso Latinoamericano de Geología. Asociación Geológica Argentina, Buenos Aires, pp. 3.

Geuna, S.E., Somoza, R., Vizán, H., Figari, E.G., Rinaldi, C.A., 2000. Paleomagnetism of Jurassic and Cretaceous rocks in central Patagonia: a key to constrain the timing of rotations during the breakup of southwestern Gondwana? Earth Planet. Sci. Lett. 181, 145–160. https://doi.org/10.1016/S0012-821X(00)00198-9.

Giacosa, R., Márquez, M., Nillni, A., Fernández, M., Fracchia, D., Parisi, C., Afonso, J., Paredes, J., Sciutto, J., 2004. Litología y estructura del basamento ígneo-metamórfico del borde SO del Macizo Nordpatagónico al oeste del río Chico, (Cushamen, Chubut, 42° 10'S - 70° 30'O). Rev. Asoc. Geol. Argent. 59, 569–577.

Giacosa, R.E., González, P.D., Silva Nieto, D., Busteros, A., Lagorio, S.L., Rossi, A., 2014. Una nueva unidad metamórfica de alto grado en el basamento de Gastre, Macizo Nordpatagónico (Chubut). Presented at the XIX Congreso Geológico Argentino, Asociación Geológica Argentina, Córdoba.

Giacosa, R.E., Silva Nieto, D., Busteros, A., Lagorio, S.L., Hernando, I., 2017. Estructura de la región Occidental del Macizo Nordpatagónico. In: XX Congreso Geológico Argentino. Asociación Geológica Argentina, San Miguel de Tucumán.

Gosen, W.V., 2009. Stages of Late Palaeozoic deformation and intrusive activity in the western part of the North Patagonian Massif (southern Argentina) and their geotectonic implications. Geol. Mag. 146, 48–71. https://doi.org/10.1017/S0016756808005311.

Hervé, F., Calderón, M., Faúndez, V., 2008. The metamorphic complexes of the Patagonian and Fuegian Andes. Geol. Acta: Int. Earth Sci. J. 6, 43–53.

Hole, M.J., Ellam, R.M., Macdonald, D.I.M., Kelley, S.P., 2016. Gondwana break-up related magmatism in the Falkland Islands. J. Geol. Soc. 173, 108–126. https://doi.org/10.1144/jgs2015-027.

Kent, D.V., Irving, E., 2010. Influence of inclination error in sedimentary rocks on the Triassic and Jurassic apparent pole wander path for North America and implications for Cordilleran tectonics. Acad. Commons 115https://doi.org/10.7916/D8ST80BZ. B10103–B10103.

Kirschvink, J.L., 1980. The least-squares line and plane and the analysis of palaeomagnetic data. Geophys. J. R. Astron. Soc. 62, 699–718. https://doi.org/10.1111/j.1365-246X.1980.tb02601.x.

Lagorio, S., Busteros, A., Silva Nieto, D., Giacosa, R., 2015. Nuevas edades U-Pb SHRIMP en granitoides del Batolito de la Patagonia Central, Gastre, Provincia del Chubut (República Argentina). In: XIV Congreso GEológico Chileno. Sociedad Geológica de Chile, La Serena, pp. 874–877.

López de Luchi, M.G., Cerredo, M.E., 2008. Geochemistry of the Mamil Choique granitoids at Rio Chico, río Negro, Argentina: late Paleozoic crustal melting in the north Patagonian Massif. J. South Am. Earth Sci. 25, 526–546. https://doi.org/10.1016/j.jsames.2007.05.004.

MacDonald, D.I.M., Gomez-Perez, I., Franzese, J., Spalletti, L.A., Lawver, L.A., Gahagan, L., Dalziel, I., Thomas, C.G.C., Trewin, N.H., Hole, M.J., Paton, D.A., 2003. Mesozoic break-up of SW Gondwana: implications for regional hydrocarbon potential of the southern South Atlantic. Mar. Pet. Geol. 20, 287–308. https://doi.org/10.1016/S0264-8172(03)00045-X.

Marshall, J.E.A., 1994. The Falkland Islands: a key element in Gondwana paleogeography. Tectonics 13, 499–514. https://doi.org/10.1029/93TC03468.

McFadden, P.L., McElhinny, M.W., 1990. Classification of the reversal test in palaeomagnetism. Geophys. J. Int. 103, 725–729. https://doi.org/10.1111/j.1365-246X.1990.tb05683.x.

Navarrete, C., Gianni, G., Encinas, A., Márquez, M., Kamerbeek, Y., Valle, M., Folguera, A., 2019. Triassic to Middle Jurassic geodynamic evolution of southwestern Gondwana: from a large flat-slab to mantle plume suction in a rollback subduction setting. Earth Sci. Rev. 194, 125–159. https://doi.org/10.1016/j.earscirev.2019.05.002.

Nullo, F.E., 1978. Descripción Geológica de la hoja 41d, Lipetren: Provincia de Río Negro, Boletin. Secretaría de Estado de Mineria, Buenos Aires.

O'Reilly, W., 1984. Rock and Mineral Magnetism. Springer, US. https://doi.org/10.1007/978-1-4684-8468-7.

Page, R., Page, S., 1994. Petrología y sugnificado tectónico del Jurásico volcánico del Chubut central. Rev. Asoc. Geol. Argent. 48, 41–58.

Proserpio, C.A., 1978. Descripción Geológica de la hoja 42d, Gastre: provincia del Chubut, Boletin. Secretaría de estado de Mineria, Buenos Aires.

Rapela, C.W., Dias, G.F., Franzese, J.R., Alonso, G., Benvenuto, A.R., 1991. El Batollto de la Patagonia Central: evidencias de un magmatismo Triasico-Jurasico asociado a fallas transcurrentes. Andean Geol. 18, 121–138. https://doi.org/10.5027/andgeoV18n2-a03.

Rapela, C.W., Kay, S., 1988. Late Paleozoic to recent magmatic evolution of northern Patagonia. Episodes 2, 175–182.

Rapela, C.W., Pankhurst, R.J., 1992. The granites of northern Patagonia and the Gastre fault system in relation to the break-up of Gondwana. Geol. Soc., Lond., Spec. Publ. 68, 209–220. https://doi.org/10.1144/GSL.SP.1992.068.01.13.

Rapela, C.W., Pankhurst, R.J., Fanning, C.M., Hervé, F., 2005. Pacific subduction coeval

with the Karoo mantle plume: the Early Jurasssic Subcordilleran belt of northwestern Patagonia. Geol. Soc., Lond., Spec. Publ. 246, 217–239. https://doi.org/10.1144/GSL.SP.2005.246.01.07.

Rapela, C.W., Pankhurst, R.J., Harrison, S.M., 1992. Triassic "Gondwana" granites of the Gastre district, North Patagonian Massif. Earth Environ. Sci. Trans. Royal Soc. Edinb. 83, 291–304. https://doi.org/10.1017/S0263593300007975.

Renda, E.M., Alvarez, D., Prezzi, C., Oriolo, S., Vizán, H., 2019. Inherited basement structures and their influence in foreland evolution: a case study in Central Patagonia, Argentina. Tectonophysics 772, 228232. https://doi.org/10.1016/j.tecto.2019.228232.

Ruiz González, V., Puigdomenech, C.G., Renda, E.M., Boltshauser, B., Somoza, R., Vizán, H., Zaffarana, C.B., Taylor, G.K., Haller, M., Fernández, R., 2019. New paleomagnetic pole for the upper Jurassic Chon Aike formation of southern Argentina (South America): testing the tectonic stability of Patagonia with respect to South America, and implications to middle Jurassic-early Cretaceous true polar wander. Tectonophysics 750, 45–55. https://doi.org/10.1016/j.tecto.2018.10.028.

Savignano, E., Mazzoli, S., Arce, M., Franchini, M., Gautheron, C., Paolini, M., Zattin, M., 2016. (Un)Coupled thrust belt-foreland deformation in the northern Patagonian Andes: new insights from the Esquel-Gastre sector (41°30′–43°S). Tectonics 35, 2636–2656. https://doi.org/10.1002/2016TC004225.

Storey, B.C., Curtis, M.L., Ferris, J.K., Hunter, M.A., Livermore, R.A., 1999. Reconstruction and break-out model for the Falkland Islands within Gondwana. J. Afr. Earth Sci. 153–163. https://doi.org/10.1016/S0899-5362(99)00086-X. Gondwana-10: Event Stratigraphy of Gondwana, Proceedings volume 1 29.

Suárez, R., González, P.D., Ghiglione, M.C., 2019. A review on the tectonic evolution of the Paleozoic-Triassic basins from Patagonia: Record of protracted westward migration of the pre-Jurassic subduction zone. J. South Am. Earth Sci. 95, 102256. https://doi.org/10.1016/j.jsames.2019.102256.

Torsvik, T.H., Van der Voo, R., Preeden, U., Mac Niocaill, C., Steinberger, B., Doubrovine, P.V., van Hinsbergen, D.J.J., Domeier, M., Gaina, C., Tohver, E., Meert, J.G., McCausland, P.J.A., Cocks, L.R.M., 2012. Phanerozoic polar wander, palaeogeography and dynamics. Earth Sci. Rev. 114, 325–368. https://doi.org/10.1016/j.earscirev.2012.06.007.

Vizán, H., Ixer, R., Turner, P., Cortés, J.M., Cladera, G., 2004. Paleomagnetism of upper Triassic rocks in the los Colorados hill section, Mendoza province, Argentina. J. South Am. Earth Sci. 18, 41–59. https://doi.org/10.1016/j.jsames.2004.08.008.

Vizán, H., Prezzi, C.B., Geuna, S.E., Japas, M.S., Renda, E.M., Franzese, J., Zele, M.A.V., 2017. Paleotethys slab pull, self-lubricated weak lithospheric zones, poloidal and toroidal plate motions, and Gondwana tectonics. Geosphere 13, 1541–1554. https://doi.org/10.1130/GES01444.1.

Volkheimer, W., 1964. Estratigrafía de la zona extrandina del departamento de Cushamen (Chubut) entre los paralelos 42º y 42º 30' y los meridianos 70º y 71º. Rev. Asoc. Geol. Argent. 19, 85–107.

von Gosen, W., Loske, W., 2004. Tectonic history of the Calcatapul Formation, Chubut province, Argentina, and the "Gastre Fault system". J. South Am. Earth Sci. 18, 73–88. https://doi.org/10.1016/j.jsames.2004.08.007.

von Gosen, W., Loske, W., Prozzi, C., 2002. New isotopic dating of intrusive rocks in the Sierra de San Luis (Argentina): implications for the geodynamic history of the Eastern Sierras Pampeanas. J. South Am. Earth Sci. 15, 237–250. https://doi.org/10.1016/S0895-9811(02)00016-0.

Wilson, R.L., Dagley, P., McCormack, A.G., 1972. Palaeomagnetic evidence about the source of the geomagnetic field. Geophys. J. Int. 28, 213–224. https://doi.org/10.1111/j.1365-246X.1972.tb06124.x.

Zaffarana, C., Gallastegui, G., Lagorio, S., Poma, S., Busteros, A., Serra Varela, S., Orts, D., Silva Nieto, D., Giacosa, R., Ruiz González, V., Puigdomenech, C., Boltshauser, B., Somoza, R., 2018a. Geochemical signature and reservoir conditions of early Jurassic calc-alkaline volcanic rocks from Lonco Trapial Formation, central Patagonia. J. South Am. Earth Sci. 88, 415–445. https://doi.org/10.1016/j.jsames.2018.09.006.

Zaffarana, C., Lagorio, S., Orts, D., Busteros, A., Nieto, D.S., Giacosa, R., González, V.R., Boltshauser, B., Negre, C.P., Somoza, R., Haller, M., 2018b. First geochemical and geochronological characterization of Late Cretaceous mesosilicic magmatism in Gastre, Northern Patagonia, and its tectonic relation to other coeval volcanic rocks in the region. Geol. Mag. 1–10. https://doi.org/10.1017/S0016756818000432.

Zaffarana, C.B., 2011. Estudio de la Deformación Pre-Cretácica en la Región de Gastre, Sector sur del Macizo Norpatagónico. Universidad de Buenos Aires, Buenos Aires.

Zaffarana, C.B., López de luchi, M.G., Somoza, R., Mercader, R., Giacosa, R., Martino, R.D., 2010. Anisotropy of magnetic susceptibility study in two classical localities of the Gastre Fault System, central Patagonia. J. South Am. Earth Sci. 30, 151–166. https://doi.org/10.1016/j.jsames.2010.10.003.

Zaffarana, C.B., Montenegro, T., Somoza, R., 2012. The host rock of the central Patagonian batholith in Gastre: further insights on the late Triassic to early Jurassic deformation in the region. Rev. Asoc. Geol. Argent. 69 0–0.

Zaffarana, C.B., Somoza, R., 2012. Palaeomagnetism and 40Ar/39Ar dating from Lower Jurassic rocks in Gastre, central Patagonia: further data to explore tectonomagmatic events associated with the break-up of Gondwana. J. Geol. Soc. 169, 371–379. https://doi.org/10.1144/0016-76492011-089.

Zaffarana, C.B., Somoza, R., López de Luchi, M., 2014. The late Triassic central Patagonian batholith: Magma hybridization, 40Ar/39Ar ages and thermobarometry. J. South Am. Earth Sci. 55, 94–122. https://doi.org/10.1016/j.jsames.2014.06.006.

Zaffarana, C.B., Somoza, R., Orts, D.L., Mercader, R., Boltshauser, B., González, V.R., Puigdomenech, C., 2017. Internal structure of the late Triassic central Patagonian batholith at Gastre, southern Argentina: implications for pluton emplacement and the Gastre Fault system. Geosphere 13, 1973–1992. https://doi.org/10.1130/GES01493.1.